Chapter Number (18pt)

Ultrafast spatiotemporal laser pulse engineering using chromatic dispersion

Yuelin Li
Argonne National Laboratory, Argonne, IL 60439
USA

1. Introduction

Tailoring the geometry of a laser pulse is one of the important fields of laser research and application. The most common form of a laser pulse is a Gaussian distribution in all dimensions. Transversely, this is the solution of the paraxial Helmholtz wave equation. A Gaussian distribution is invariant under Fourier transforms in both transverse and longitudinal dimensions.

Many applications only require shaping the transverse irradiance profiles. Those include material processing, medical procedures, lithography, and optical data processing (Dikey & Holswade, 2000), mostly to generate a flat-top, homogeneous intensity distribution. A variety of aspheric optics designs exist to convert a Gaussian beam into a flat top beam (Dikey & Holswade, 2000; Hoffnagle & Johnson, 2000; Zhang, Neil, & Shinn, 2003).

Precise, high-fidelity temporal shaping is demanded in applications such as coherence control in quantum systems, optical signal processing, and laser-matter interaction for ultrafast electron and radiation sources and is made possible by the advent of ultrafast lasers (Weiner, 1995). Weiner (Weiner, 1995) has given a comprehensive review of available techniques. The two main techniques are the spatial light modulator (SLM) (Weiner, 2000) and the acousto-optic programmable dispersive filter (AOPDF) (Verluise et al., 2000), which allows phase and amplitude tailoring in the time and frequency domain in a ps or fs time.

Spatiotemporal control is intrinsically complex due to the difficulty in simultaneously controlling the spatial and temporal distribution. Examples of successful high-fidelity shaping are sparse. The techniques include the use of 2-D SLM to shape the waveform of the pulse at different spatial locations in a 2-D manner (Vaughan et al., 2002), or the use of the spatial temporal duality of light by transforming a 2-D holographic image into a 2-D spatial temporal distribution (Nuss and Morrison, 1995). Three-dimensional control thus far has only been achieved via structured optics (Piestun & Miller, 2001), or temporal multiplexing via volume holography (Hill, Purchase & Brady, 1995).

One of the important applications for multiple dimension control of a laser pulse is for high-brightness electron beam generation in a photoinjector. This is critical for cost effective X-ray free electron lasers (Brinkmann et al., 1997; Cornacchia et al. 1998) and other beam based light sources (Grunner et al., 2002), as well as ultrafast electron beam imaging and diffraction experiment (King et al., 2005). To this end, viable solutions for a homogeneous

cylindrical beam have been developed using a combination of transverse shaping and temporal phase control, or with pulse stacking using multiple delay optics (Sider, 1998; Tomizawa et al., 2006) and birefringence crystals (Dromey et al., 2007; Will & Klemz 2008; Bazarov, Ouzounov& Dunham, 2008; Sharma, Tsang & Rao, 2009).

For the more desirable homogeneous ellipsoidal beam shape due to totally linear space charge force (Reiser, 2005), pulse stacking becomes very complicated, though theoretically still possible, for example, via temporal multiplexing via volume holography (Hill, Purchase & Brady, 1995). The drawback, besides the low efficiency, is the volatility of the hologram media, which degenerates during readout (Brady & Psaltis, 1992).

In this chapter, we will discuss a new way of controlling the spatiotemporal distribution of photons via the well known chromatic dispersion in an optical system (Li and Lewellen, 2008; Li & Chemerisov, 2008; Li, Chemerisov & Lewellen, 2009). Normally, such effect causes adverse effects that distort both the temporal and the spatial fidelity of a laser pulse. In space, this gives rise to chromatic aberration, i.e., light of different wavelength will focus at different distance from the lens. For ultrashort pulses, significant lengthening of the pulse has been predicted and observed (Bor, 1989; Bor & Horvath, 1992; Kempe et al., 1992).

However, due to the wavelength and phase dependence of the chromatic dispersion, pulse engineering is possible by coupling the space and time domain properly using available time and frequency domain phase- and amplitude- tailoring techniques.

We will start with a discussion of the chromatic aberration and its coupling to the time domain phase in a singlet lens, followed by Fourier optics of a laser pulse transmitted through a singlet lens with examples of temporal distortion due to chromatic dispersion for pulse with and without nonlinear phases. We will then give an example of using the aberration-phase coupling for an ellipsoidal pulse generation together with a proof-of-principle experiment. Future work will also be addressed.

2. Formulation of chromatic dispersion in an optical singlet lens

2.1 Chromatic aberration in Gaussian optics

Chromatic dispersion is the phenomenon in which the phase velocity and group velocity of a wave depends on its frequency, arising from the dependence of the refractive index upon the optical frequency (Born & Wolf, 2003).

Chromatic dispersion, as a function of frequency, manifested itself into space as chromatic aberration in an optical lens, where light with different frequency focuses at different location. For a thin, singlet spherical lens in air, the focal length f is

$$\frac{1}{f} = [n(\omega) - 1]\left(\frac{1}{R_1} - \frac{1}{R_2}\right), \tag{1}$$

where R_1 and R_2 are the radius of curvature for the entrance and exit side of the lens, respectively, $n(\omega)$ is the frequency- or wavelength-dependent refractive index of the lens material. From Eq. (1), the change of the focal length due to a shift in frequency $\delta\omega$ is

$$\delta f = -\frac{f_0}{n_0 - 1}\beta\delta\omega \ , \tag{2}$$

where f_0 is the nominal focal length at ω_0. We assume a constant $\beta = dn/d\omega$ for this analysis. At the nominal focal plane for ω_0, this leads to a defocused beam or a larger focus size. In Gaussian optics, this new focus size can be easily calculated,

$$w \approx w_0\left[1+\left(\frac{\delta f}{z_R}\right)^2\right]^{1/2} = w_0\left[1+\left(\frac{1}{z_R}\frac{f_0}{n_0-1}\beta\delta\omega\right)^2\right]^{1/2}. \quad (3)$$

Here $w_0=N\lambda_0/\pi$ is the beam waist at the nominal wavelength λ_0, with N the numerical aperture, and $z_R=\pi w_0^2/\lambda_0$ is the Rayleigh range. Note that both the beam waist and the Rayleigh length are a function of the wavelength. However, in our analysis, the effect is small and is henceforth ignored.

It is obvious from Eqs. (2) and (3) that if one can program $\delta\omega$ in time, a programmable time-dependent beam size can be achieved at certain focal plane. At $\delta f >> z_R$, one has,

$$w(t) \approx w_0 \frac{1}{z_R}\frac{f_0}{n_0-1}\beta\delta\omega(t). \quad (4)$$

For a given $w(t)$, the needed phase of the laser pulse can be obtained as

$$\phi(t) = \pm\int \delta\omega(t)dt = \pm\frac{n_0-1}{\beta}\frac{N}{f_0}\int w(t)dt. \quad (5)$$

For a desired time-dependent intensity $I(t)$, the amplitude of the laser should be

$$a(t) \propto I(t)^{1/2} w(t). \quad (6)$$

This is an example of how behaviour in time and space can be coupled, and it is only made possible though the manifestation of chromatic dispersion into chromatic aberration. This forms the theoretical base for our spatiotemporal shaping method.

As can be seen below, the final result is also significantly affected by the time domain effect and certain diffraction due to the apodization of the beam.

2.2 Time domain effects using Fourier optics

The above discussion is based on geometry and Gaussian optics, where the effect due to dispersion is only considered in the space domain. As dispersion is mainly due to dependence of group and phase velocity on frequency, thus the primary effect is in the time domain.

To treat the time domain effect, we base our discussion on the Fourier optics formula for a dispersive singlet lens elaborated by Kempe et al. (Kempe et al., 1992):

$$U(r,\omega) = \int_0^P \rho d\rho \int_0^{2\pi} d\theta A(\rho,\omega)\Gamma_1(\rho,\omega)\exp\left(-jk_a\sqrt{f_0^2+\rho^2+r^2-2\rho r\cos\theta}\right), \quad (7)$$

$$\Gamma_1(\rho,\omega) = \exp(jk_l d)\exp\left[-j(k_l-k_a)\frac{\rho^2}{2(n-1)f_0}\right] \quad (8)$$

Here U is the frequency domain representation of the field at the focal plane, f_0 is the nominal focal length of the lens. Here $A(\rho,\omega) = F[a(\rho,t)\exp(-j\phi(t))]$ is the Fourier transform of the input pulse; and P, ρ, and θ are the lens radius or beam aperture, the ray entrance location from the axis, and the azimuthal angle, respectively. Γ_1 is the lens transfer function, with k_l and k_a the wave numbers in the lens and air, respectively. Γ_1 derives its ρ-dependence from the thickness variation of the lens across the beam aperture. For a flat top input beam, at the focal plane of the lens and on axis at r=0, Eq. (7) can be rewritten as

$$U(\omega) = 2\pi\int \rho d\rho A(\omega)\Gamma(\rho,\omega), \quad (9)$$

$$\Gamma(\rho,\omega) = \exp\left(jk_l d + j\frac{k_a}{2f_0}\rho^2\right)\exp\left[-j(k_l-k_a)\frac{\rho^2}{2(n-1)f_0}\right]. \quad (9a)$$

The time domain field can be obtained by an inverse Fourier transform of Eq. (9),

$$u(t) = 2\pi \int \rho d\rho a * \gamma \cdot \tag{10}$$

Where the symbol * represents convolution, with $\gamma = \gamma(\rho, t) = F^{-1}\,\Gamma(\rho, \omega)$, respectively. Here F^{-1} denotes inverse Fourier transformation.

Following the elaboration in Kempe et. al. (Kempe et al., 1992) and ignoring the constant phase terms, we obtain from Eq. (9a) for $\Delta\omega = \omega - \omega_0$,

$$\Gamma(\rho, \omega) = \exp\left[jk\left(\beta T \Delta\omega + n_0 \chi T \Delta\omega^2\right)\right], \tag{11}$$

with

$$T(\rho) = d - \frac{\rho^2}{2(n_0 - 1) f_0},\ \beta = \frac{dn}{d\omega},\ \ \chi = \beta \frac{1}{\omega} + \frac{1}{2}\frac{d^2 n}{d\omega^2}.$$

Here d is the thickness of the lens center at $\rho = 0$. Thus we have

$$\gamma(\rho, t) = F^{-1}\Gamma(\rho, \omega) = \frac{1}{2\sqrt{k n_0 \chi T}} \exp\left[j \frac{(t - k\beta T)^2}{4 k n_0 \chi T} \right]. \tag{12}$$

For a Gaussian input pulse,

$$a(t) = a_0 \exp\left[-2 \ln 2 \left(\frac{t}{\tau} \right)^2 \right], \tag{13}$$

where τ is the full width at half maximum (FWHM) of the pulse, we obtain from Eqs. (10) – (12),

$$u(t) = 2\pi a_0 \int \rho d\rho \frac{1}{\left(1 + \Lambda^2\right)^{1/4}} \exp\left[-2 \ln 2 \frac{(t - k\beta T)^2}{\tau^2 (1 + \Lambda^2)} (1 - j\Lambda) \right] \exp\left[j \tan^{-1}(-\Lambda) \right], \tag{14}$$

with

$$\Lambda = \frac{4 k n_0 \chi T}{\tau^2} \cdot \tag{15}$$

In comparison with the input pulse, Eq. (14) shows two effects. The first is the group velocity delay (GVDE), which causes the pulse originate at different radial location to arrive at the focus at different time characterized by $T(\rho)$ and has a quadratic dependence on the radius ρ of the entrance position. For short pulses, this leads to time broadening as first discussed by Bor (Bor, 1989).

The second effect is the common group velocity dispersion (GVDI), i.e., light waves with different frequencies propagate at different group velocities in a dispersive medium, which also leads to lengthening of the pulse.

An interesting example is when the input pulse has a significant time/envelope dependent nonlinear phase such as a third order phase due to self-phase modulation (SPM) or B-integral (Li & Crowell, 2007). As we will see, this is the regime where our spatiotemporal shaping method resides, as described by Eqs (5) and (6).

We assume that the pulse has a small enough bandwidth, hence the second order terms in Eq. (7) can be neglected, therefore

$$\gamma(\rho, t) = \delta\left(t - k\beta T\right), \tag{16}$$

and the nonlinear Schrodinger equation (NLSE) (Agrawal, 1995) governing the propagation of a laser pulse in a nonlinear medium can be analytically solved to give the pulse right after the lens as,

$$a(\rho,t) = a_0 \exp\left(-2\ln 2\frac{t^2}{\tau^2}\right)\exp\left[j\mu\exp\left(-4\ln 2\frac{t^2}{\tau^2}\right)\zeta\right], \quad (17)$$

$$\mu = kn_2 a_0^2 d.$$

Here ζ is a phase modulation parameter, $\zeta=T/d$ if the SPM is generated in the lens and $\zeta=L/d$ if the self modulated phase is accumulated before arriving at the lens through an effective beam path of L. The pulse at the focus is then

$$u(t) = a_0 \int \rho d\rho \exp\left(-2\ln 2\frac{(t-k\beta T)^2}{\tau^2}\right)\exp\left[j\mu\exp\left(-4\ln 2\frac{(t-k\beta T)^2}{\tau^2}\right)\zeta\right]. \quad (18)$$

We can see that similar to Eq. (14), the integrand in Eq. (18) shows that the field at the focus is the superposition the of pulse slices with shifted arriving time. However, the temporal dependence of the phase now causes the superposition to be either constructive or destructive, and in general with small enough μ, shortened the pulse. This is depicted in Figs. 1 (a) and (b), showing the real part of the integrand in Eq. (18) as a function of t and ρ. The drifting of the field pattern as function of ρ is clear resulting into shortened pulses $u(t)$, as shown in Figs. 1 (c) and (d). The pulses are shortened to 0.21 ps and 0.2 ps from that of the input pulse of 1 ps for $\zeta=T/d$ and $\zeta=L/d=1$, respectively, a factor of 5 in reduction. In the calculation, we use a fused silica lens of f_0=150 mm, d=5 mm, and an aperture of P=12 mm in radius. The laser wavelength is 249 nm. An intensity of 5×10^{11} W/cm^2 is used resulting into a μ=15 rad. We use an $n_2=2.38\times10^{-16}$ W/cm^2 (Taylor, Rodriguez & Clement, 1996). This pulse shortening is in contrast to the lengthening effect discussed by previous authors (Bor, 1989;

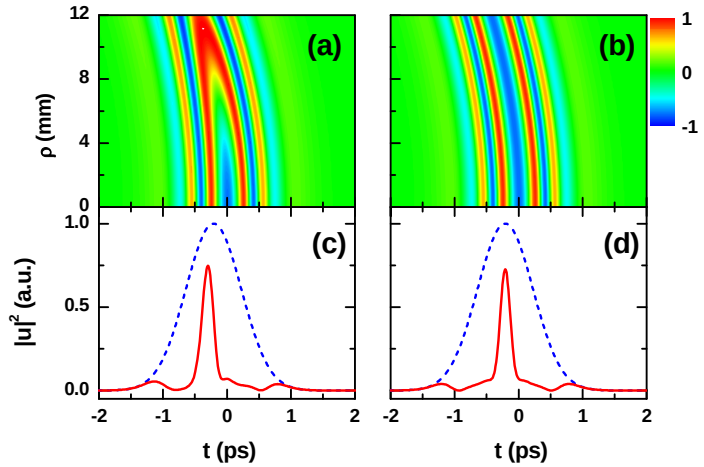

Figure 1 The real part of the complex field at the focus as a function of time and radius for $\zeta=T/d$ (a) and $\zeta=1$ (b), and the corresponding the intensity of the integrated field (solid) and the input pulse (dashed) as a function of time for the same cases [(c) and (d)]. The input pulse is shortened from 1 ps to 0.21 (c) and 0.20 ps (FWHM) (d) at the focus, a reduction by a factor of 5. The calculation assumes an f=150 mm lens with P=12 mm and d=5 mm. The laser wavelength is 249 nm with μ=15 at a laser intensity of 5×10^{11} W/cm^2.

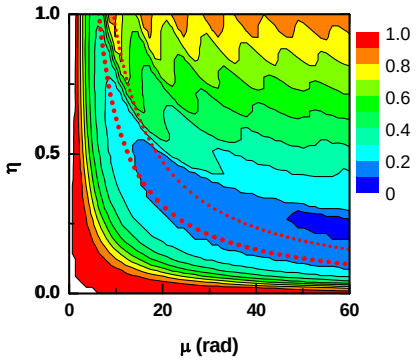

Fig. 2 Output/input pulse duration ratio as a function of time shift parameter η and the phase shift parameter μ for a τ=1 ps Gaussian pulse for ζ=1. The two dotted lines are $\eta\mu$=2π and 3π. Calculation for pulse duration ranging up to a few nanoseconds gives identical distributions.

Bor & Horvath, 1992; Kempe et al., 1992). Under the same condition, a 50 fs pulse would be stretched to 0.5 ps without the SPM. Because of the similarity, we limit our discussion for cases with ζ=1 in the following.

As the pulse shortening is due to localized destructive superposition of the field, first, the phase slip between the pulse slices should be bigger enough so that destructive superposition dominates and, second, the phase slippage should be small enough so that the phase span is limited and the final pulse will not become the sum of a set of quasi random phaser, which will result in a thermal light (Goodman, 1985). Let the group delay between the center and edge be Δt, the above statement can be expressed as $\Delta t\mu/\tau \approx$ constant, or

$$\eta\mu \approx \text{constant}, \tag{19}$$

with

$$\eta = \frac{\beta R^2}{2(n_0 - 1) f_0 \tau} = \frac{1}{N} \frac{\beta \mathrm{P}}{\tau} \ . \tag{20}$$

The scaling in Eq. (20) is qualitatively demonstrated in Fig. 2, where the ratio of the FWHM at the focus to that of the input pulse is plotted as a function of η and μ, where the maximum shortening centers around $\eta\mu$=2π -3π. Although the plot in Fig. 2 is for an input pulse duration of 1 ps, it is verified that it is universal and covers for a large range of input pulse duration from a few fs to several ps if the GVDI is ignored.

To gain more insight, a set of numerical integration for Eq. (7) is carried out with SPM effect included in the input pulse and with GVDI in the lens considered. Fig. 3 (a) shows the on-axis pulse envelope as a function the distance from the focus. In Fig. 3 (b-c), the intensity distribution as a function of radius and time of the 1 ps pulse at the focus are compared with and without SPM. Clearly, the pulse is significantly shortened and maintains its short duration in a large space range, and its spatial fidelity is well maintained. The rest of the pulse is "scattered" away from the focal region due to the wavefront distortion.

It should be mentioned that, the modulated phase can also be acquired through cross phase modulation (XPM) when multiple laser beams overlaps in time and space in the same medium, and can be more severe than SPM.

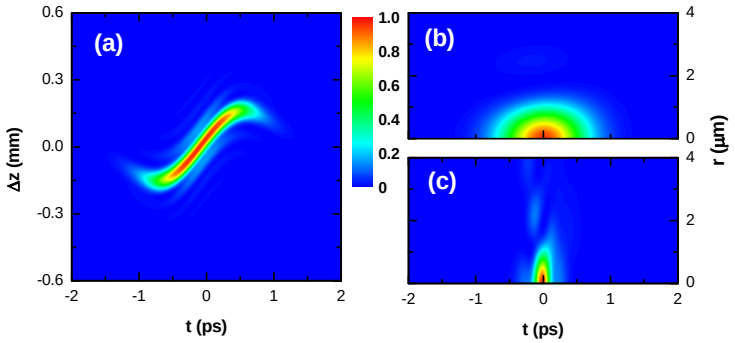

Fig. 3 (a) On axis laser pulse envelope as a function of the distance from the focus and temporal and spatial distribution of focus for SPM shortened pulse (b) and a pulse without SPM effect (n_2=0) (c). The calculation assumes an f_0=150 mm lens with P=12 mm and d=5 mm, μ=15 at laser intensity of 5×10^{11} W/cm^2.

Note that Eq. (18) is valid only when A^2 <<1 for both input pulse and the pulse with the modulated phase, this eventually limits the initial pulse duration, the medium length, and the laser pulse intensity. The laser intensity is in addition limited by the damage threshold of fused silica, which is a few times of 10^{12} W/cm^2 (Stuart et al., 1995; Tien et al., 1999). For the examples in this chapter, the validity is checked by solving the NLSE (Agrawal, 1995) numerically.

This pulse shortening due to SPM is only one of the examples how dispersion can affect the performance of an optical lens and needs to be carefully examined for many applications involving manipulating intense UV beams, such as focusing the multi kilo joule UV laser beam into a holrum in inertial confinement fusion experiments and in shaping and delivering an high quality UV pulse for a modern photoinjector which we will discuss below. In those applications the modulated phase may accumulate duration the laser transport and frequency conversion. The remedy is to use achromatic optics when possible, which has been shown to be effective in mitigate the pulse lengthening effect.

3. Application to ultrafast, spatiotemporal pulse engineering: a light ellipsoid

3.1 Numerical results

Though the potential of using Eqs. (5) and (6) for designed spatiotemporal shaping is unlimited, a practical example of the spatiotemporal shape is the uniform ellipsoidal (UE) pulse desired for modern photoinjectors (Reiser, 1995; Li & Lewellen, 2008; Limborg_Depray & Bolton, 2006) to generate high brightness electron beams. Such beam profile provides the possibility of maximizing the beam brightness with high efficiency suitable for more cost effective X-ray free-electron lasers and other electron beam-based light sources (Brinkmann et al., 1997; Cornacchia et al. 1998; Grunner et al., 2002). The envelope of the beam is defined by an ellipsoid surface

$$R(t) = R_0\sqrt{1-(t/\Theta)^2}\,. \tag{21}$$

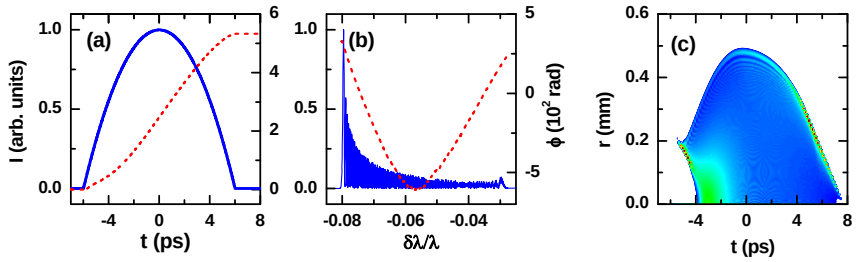

Fig. 4 Time and (b) frequency domain representation (solid line: intensity; dashed line: phase), and (c) the spatiotemporal intensity distribution of a laser pulse that gives an excellent emittance performance in beam simulation [α=1/2 at t<0, α=1 at t≥0, and ξ=1/2 in Eqs. (22) and (23)]. The pulse has a 5% full bandwidth at 249 nm (about 1% full width at half maximum). A P=25 mm and f_0=150 mm fused silica lens is used. The spatiotemporal distribution in (c) represents the laser pulse to be applied to the cathode.

Here 2Θ is the full temporal width and R_0 the maximum radius. Within the envelope, the electron distribution should be homogeneous and outside the envelope, there should be no electrons at all. The scheme for generating such an electron distribution via dynamic self evolution (Luiten et al., 2004; Musumeci et al., 2008) is limited to low charge cases (Li & Lewellen, 2008), thus to generate an ellipsoidal laser beam remains the ultimate solution and challenge.

To generate an ellipsoidal envelope described by Eq. (21), substitute $w(t)$ with $R(t)$ in Eq. (5), the desired phase becomes,

$$\phi(t) = -\omega_0 t \pm \frac{\Delta\omega}{2}\left[t\left(1-\left(\frac{t}{\Theta}\right)^2\right)^{\alpha} + \Theta\sin^{-1}\frac{t}{\Theta}\right], \tag{22}$$

where α=1/2, and $\Delta\omega$=$(n_0$-$1)NR_0/\beta f_0$ is the maximum frequency shift. To keep the laser flux $|a(t)|^2/R(t)^2$ constant over time, we have

$$a(t) = a_0\left[1-\left(\frac{t}{\Theta}\right)^2\right]^{\xi}, \tag{23}$$

with ξ=1/2. Equations (22) and (23) describe a pulse that can form a spatiotemporal ellipsoid at the focus of a singlet lens.

As mentioned earlier, Gaussian optics method is used to obtain Eqs. (5) and (6), thus Eqs. (22) and (23) does not treat the effects of diffraction due to beam apodization and the time domain effect of dispersion described in Sec. 2.2. These effects are numerically evaluated using a Fourier optics model described by Eqs. (7) and (8).

In fact, the group delay and diffraction effects prevent us from generating a perfect UE pulse, thus α and ξ in Eqs. (22) and (23) are adjusted for better emittance in accordance with the particle simulation (Li & Lewellen, 2008; Li, Chemerisov & Lewellen, 2009). The time and frequency domain representations of a pulse with excellent emittance performance are shown in Figs. 4 (a) and (b), with Θ=6 ps, λ_0 =0.25 μm, and $\Delta\omega/\omega$=8%. The spatiotemporal flux at the focal plane of an f_0=150 mm fused silica lens is given in Fig. 4 (c). In particle

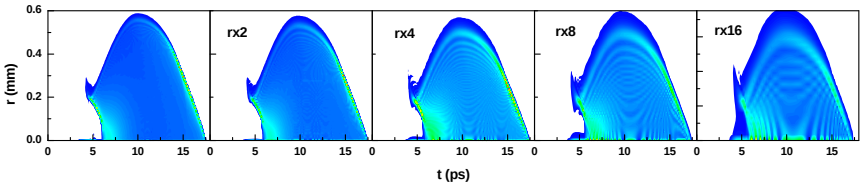

Fig. 5 Numerically calculated spatiotemporal laser profiles with different input bandwidth with P=25 mm input beam (flat topped) using the same α and ξ as in Fig. 4(c). From left to right: $\Delta\omega/\omega$=8%, 4%, 2%, 1%, and 0.5%. Note the different scales in r as noted in each panel.

tracking simulation, the emittance performance of the beam was found to closely mimicking that of an ideal ellipsoidal beam (Li & Lewellen, 2008; Li, Chemerisov & Lewellen, 2009).

The intensity in Fig. 4 (c) displays the basic features of a UE pulse but with noticeable distortions. The distortion has three components representing three different physics, which can be more clearly observed in the dependence of the spatiotemporal profile on the laser and lens parameters in Figs. 5 and 6. Figure 5 shows simulated spatiotemporal profiles of the laser pulse as a function of the laser bandwidth $\Delta\omega/\omega$= 8%, 4%, 2%, 1% and 0.5% with a lens radius of P=25 mm. Figure 6 shows profiles as a function of the lens radius P at a fixed bandwidth $\Delta\omega/\omega$= 8%.

The first effect is the group velocity delay effect shown in Eq. (14), which generates the prominent recess in the leading edge and the protrusion at the trailing edge. This is due to the group delay between rays traversing the lens at different radii, with the maximum delay determined by the lens parameters. With longer pulses, or smaller beam aperture, the impact can be much reduced, as can be seen in Fig. 6.

The second effect is the obvious diffraction fringes, mostly clear at smaller beam apertures. The detail of the diffraction structure depends on the laser bandwidths and other factors (Figs. 5 and 6). Even in this application the effect is detrimental and needs further analysis, this complicated diffraction patter can provide another dimension for spatiotemporal control of the pulse. Using apodization to manipulate the depth of focus was explored decades ago (Welford, 1960) and the effect of apodization of an ultrafast laser pulse remains an interesting research topic (Veetil, 2006).

The third effect is that is discussed in Section 2.2, the temporal modulation due to

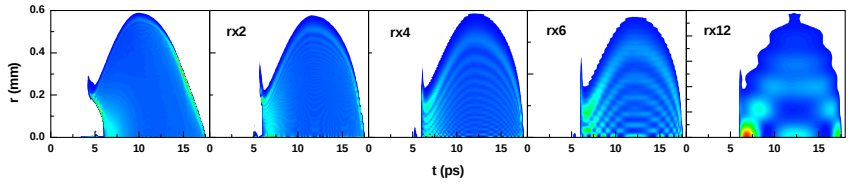

Fig. 6 Numerically calculated spatiotemporal laser profiles with different input beam size (flat topped) using the same α and ξ as in Fig. 1(c). From left to right: P=25, 12, 6, 4, and 2 mm. Note the different scales in r as noted in each panel.

superposition of the field with different phase, originating form the time-dependent phase of the input pulse.

As expected, as the bandwidth decreases, the maximum radius of the beam decreases proportionally, and the diffraction structure becomes more dominant. Smaller beam size the also makes diffraction more dominant. Though the effect on the beam needs to be evaluated further, it is clear that larger beam size and larger bandwidth is preferred.

The 3-D distribution can in general be image-relayed using achromatic optics to maintain the temporal-spatial fidelity, and the associated dispersion can be pre-compensated, as can be seen in the proof-of-principle experiment in the next section.

3.1 Experiment and results

The phase in Eq. (22), though apparently complex, is dominated by the common third order phase that can be generated via self-phase/cross phase modulation and is exploited in various laser applications, especially in few cycle pulse generation for the large bandwidth it generates during propagation. For a precise control, one of the practical solutions is the acousto-optic programmable dispersive filter (AOPDF) (Verluise et al., 2000). AOPDF uses the transient Bragg effect in a crystal induced by an acoustic wave to manipulate the phase and amplitude of a laser pulse.

A proof-of-principle experiment is carried out. A schematic of the experiment is shown in Fig. 7. A pair of Pockel cells is used to reduce the repetition rate of a Ti: Sa oscillator from 90 MHz to 1 kHz. The 40-nm bandwidth pulse is stretched to135-fs after the Pockel cells. It is split into two arms. One traverses a delay line to serve as a probe beam. The other, denoted as the main beam, is sent through an AOPDF and is modulated in phase and amplitude. It is then spatially filtered to generate a Gaussian beam using a pair of achromatic lenses and a pinhole. A plano-spherical ZnSe lens (25-mm diameter, 88.9-mm radius of curvature, and 2.9-mm center thickness, Janos Technology, A1204-105) is used for its high dispersion (250 fs^2/mm at 800 nm) to form the desired spatiotemporal distribution at its focal plane. The focal plane is image-relayed by an achromatic lens onto a CCD camera to interfere with the probe beam. The interference fringes as a function of delay between the two beams are recorded on a 12-bit camera and are used to extract the spatiotemporal intensity distribution of the main beam. The imaging system is aligned to focus at 845 nm, accomplished by generating an 845-nm beam via the AOPDF.

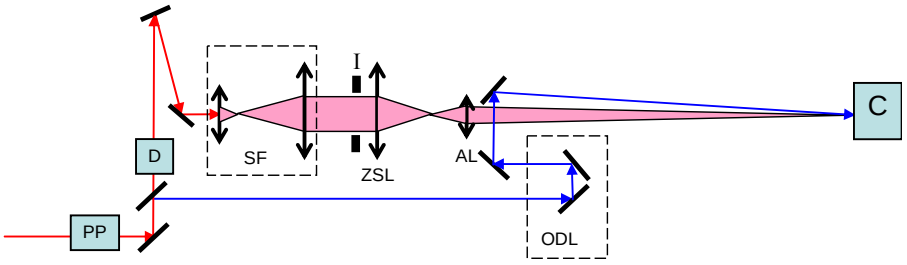

Fig. 7 Schematic of the experiment. Keys: PP: pulse picker; D: DAZZLER; SF: achromatic spatial filter; ZSL: ZnSe lens; AL: achromatic image relay lens; ODL: optical delay line; C: camera. I: iris.

For the delay scan, the AOPDF is set up according to Eqs. (4) and (5), with Θ=1 ps and a full bandwidth from 845 nm to 790 nm. The spectrum modulation function is calculated using the native spectrum of the laser to generate those specified by Eqs. (22) and (23). At the focus of the ZnSe lens, this pulse is expected to generate a tightly focused spot at the beginning and end of the pulse, but be defocused between the ends. Unless specified, all the second-order dispersion in the optics, including the third- and fourth-order dispersion in the AOPDF crystal, are canceled by properly setting the AOPDF. The calculated amplitude and phase in the time and frequency domains are given in Figs. 8 (a, b), together with a spectrum measured in the experiment. Although the measured spectrum closely matched the theoretical one, some deviation is evident and is expected due to the limited crystal length and slightly nonlinear response across the spectrum of the AOPDF. The transverse beam profile is given in Fig. 8 (c) with a $1/e^2$ radius of 6 mm. To avoid potential saturation effect of the AOPDF, the power level is set at 20%. Figure 9 shows the spectrum at several power settings of the AOPDF where the variation is clearly visible.

To extract the spatiotemporal intensity of the main beam, we start with the signal recorded

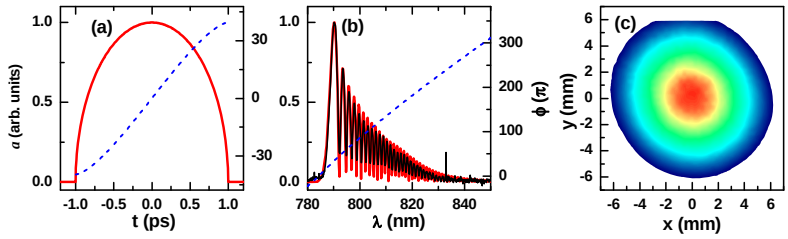

Fig. 8 Laser pulse amplitude a (bold solid lines) and phase ϕ (dashed lines) calculated from Eqs. (5) and (6) for $\alpha = \xi = 1/2$ in the time (a) and frequency (b) domains, and the measured spectrum amplitude (thin solid line in (b)). The transverse profile of the laser pulse after the spatial filter and before the ZnSe lens is shown in (c) with a slight asymmetry.

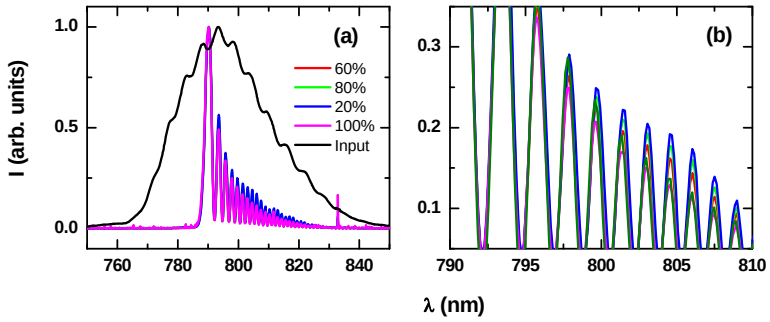

Fig. 9 (a) Variation of measured spectra as functions of AOPDF settings and (b) the detail of (a) from 790-810 nm. The target spectrum is the same as in Fig. 8 (b), with power level of AOPDF adjusted as noted in the figure. The dark green curve is the target spectrum.

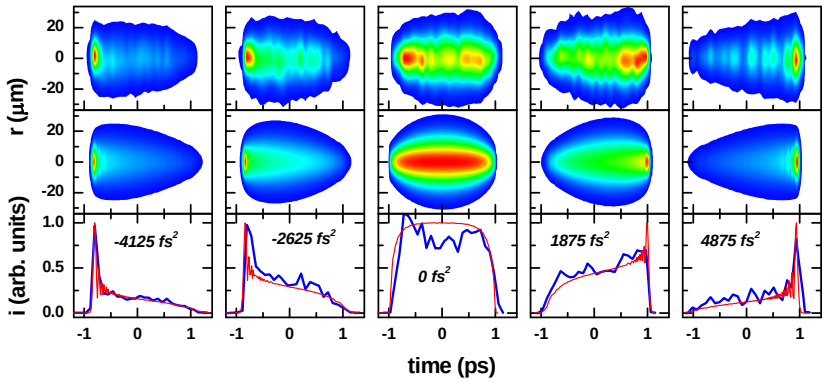

Fig. 10. Measured (top row), simulated (middle row) spatiotemporal distributions with different linear chirp in the main beam, and the intensity as a function of time at r=0 (bottom row; measured: bold lines; simulated: thin lines). Striations in the experiment data are due to the fluctuation of the laser pointing.

on the camera:

$$I(\boldsymbol{r}) = I_m(\boldsymbol{r}) + I_p(\boldsymbol{r}) + 2\cos\left(\omega[\tau + \delta(\boldsymbol{r})]\right)\int a_m(t,\boldsymbol{r})a_p(t-\delta(\boldsymbol{r})-\tau,\boldsymbol{r})\cos\left[\psi_m(t)-\phi_p(t-\delta\psi(\boldsymbol{r})-\tau)\right]dt. \quad (24)$$

where $a(t, r)$, $\psi(r)$, and I are the amplitude, phase, and integrated intensity of the laser beams; the subscripts m and p denote the main and probe beam, respectively; τ is the delay; and $\delta\psi$(r) is the phase variation due to the angle between the two laser beams. The phase term in the integral, though impossible to evaluate for each location, only causes the interference fringes at the detector to shift. Therefore, if the probe pulse is much shorter than the main pulse, Eq. (24) can be reduced to

$$I(\boldsymbol{r}) \approx I_m(\boldsymbol{r}) + I_p(\boldsymbol{r}) + 2\cos\left(\omega[\tau + \delta(\boldsymbol{r})]\right)\sqrt{\Delta t_p i_m(\tau,\boldsymbol{r})}\sqrt{I_p(\boldsymbol{r})}. \quad (10)$$

Here Δt_p is the duration of the probe pulse, and i_m is the time-dependent intensity distribution. The second term describes the fringes as functions of delay and location, from which one can extract the contrast ratio C(τ, r), which in turn gives

$$i_m(\tau,\boldsymbol{r}) \propto C^2(\tau,\boldsymbol{r})/I_p(\boldsymbol{r}). \quad (11)$$

Two sets of experiments were performed. In the first set, while maintaining the spectrum, we control the linear chirp of the main pulse using the AOPDF. Due to the specific phase of the pulse, this change will shift the "waist" (the fattest part of the spatiotemporal distribution of the beam) in time. A comparison is given in Fig. 10 between the experiment measurement and simulation with linear chirp set at different values from the fully compensated case. Other than the striations due to shot-to-shot laser fluctuation, the agreement is excellent. The input beam is a Gaussian beam with a $1/e^2$ width of 3.9 mm. No aperture is used in this part of the experiment.

The Fourier model also predicts that the fine structure of the beam is highly sensitive to the beam apodization as shown in Figs. 5 and 6. This is measured using a beam with $1/e^2$ width of 6 mm. The measured spatiotemporal intensity distributions are given in top row of

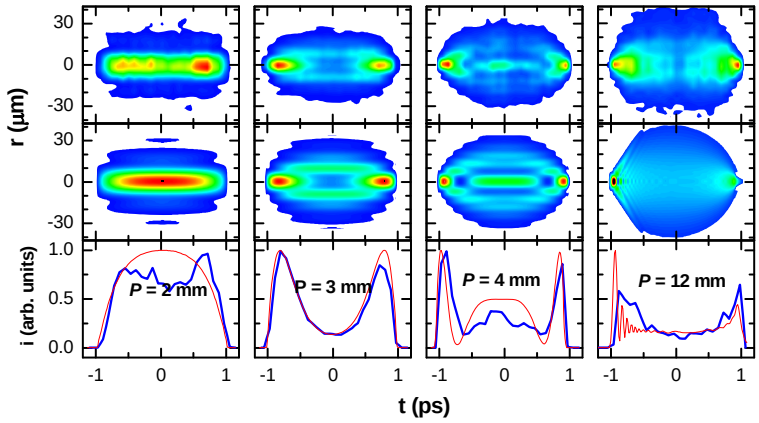

Fig. 11. Measured (top row) and simulated (middle row) spatiotemporal intensity distribution with different iris radius P using the experiment condition. The bottom row shows a comparison of the intensity at r=0 extracted from the top and middle rows (measured: bold lines; simulated: thin lines).

Figs 11. The corresponding distributions from the Fourier model are given in the middle row of Fig. 11. An iso-intensity surface plot comparison is given in Fig. 12 for the iris radius P=3 mm case. In the measurement an iris located directly in front of the ZnSe lens is adjusted to different sizes. For the measurement in Fig. 11, the second-order dispersion is set at zero.

As predicted by the Gaussian beam optics, the pulse shows generally an ellipsoidal envelope, but with dramatic variation in the internal structure due to diffraction at the iris. The diffraction pattern changes as a function of time due to both the changing wavelength and the changing focusing condition. With larger aperture size, the internal structure acquires higher and higher spatial frequency and eventually flattens out, as shown in Figs. 4 through 6.

Although the agreement between the simulation and experiment is generally good, several discrepancies can be noticed. The first is that better agreement between experiment and calculation is achieved at small aperture sizes. This can be partially attributed to the limited dynamic range of the probing system, which makes the extraction of signals difficult at low-intensity wings of the distribution. In addition, the measurement suffers from the pointing stability of the laser, which causes shot-to-shot fluctuation of both beams and thus, fluctuation of the measured intensity.

The temporal resolution of the measurement is limited by the probe pulse duration at about 130 fs; a shorter probe pulse would demand a higher dynamic range for data recording.

4. Conclusion

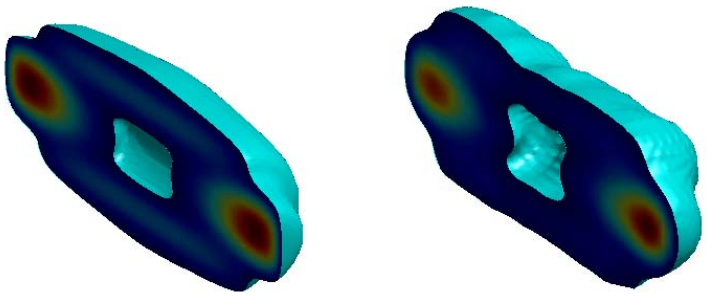

Fig. 12 Cut-away view along the *t-r* plane of the measured (right) and calculated (left) spatiotemporal iso-intensity surface plot of the P=3 mm case in Fig. 11.

We discussed the well known effect of chromatic dispersion of a singlet lens on the spatial temporal behaviour of an ultrafast laser pulse. A pulse engineering scheme exploiting these chromatic aberration is proposed with an example of generating ellipsoidal pulse for photoinjector applications. A proof-of-principle experiment was carried out with results confirming the optical Fourier model. Further investigation is planned to establish the adaptive control as well as preservation of the phase in frequency conversion. A near term goal is to demonstrate a quasi UE beam and compare it with the numerical calculation.

The authors thank K.-J. Kim and K. Harkay for support, he also thanks S. Chemerisov for assistance of the experiment and J. Lewellen for helping beam simulations. This work is supported by the U. S. Department of Energy, Office of Science, Office of Basic Energy Sciences, under Contract No. DE-AC02-06CH11357.

5. References

Agrawal, G. P. (1995). *Nonlinear Fiber Optics*, Academic Press, New York.

Bazarov, I.V. ; Ouzounov, D.G. ; Dunham, B.M. (2008). Efficient temporal shaping of electron distributions for high-brightness photoemission electron guns, *Physical Review ST AB* 11, 040702.

Bazarov, I. V. & Sinclair, C. K. (2005). Multivariate optimization of a high brightness dc gun photoinjector, *Physical Review* ST AB 8, 034202.

Born, M. & Wolf, E. (2003). *Principles of Optics*, University Press, Cambridge, UK.

Brady, D. & Psaltis, D. (1992). Control of volume holograms, *Journal of the Optical Society of America* A 9, 1167.

Bor, Z. (1989). Distortion of femtosecond laser pulses in lenses, *Optics Letters* 14, 119.

Bor, Z. & Horvath, Z. L. (1992). Distortion of femtosecond pulses in lenses. Wave optical description, *Optics Communications* 94, 249.

Brinkmann, R.; Materlik, G.; Rossbach, J. & Wagner, A. (1997), *Conceptual Design of a 500 GeV e+e- Linear Collider with Integrated X-Ray Laser Facility*, DESY Report No. DESY97-048, Deutsches Elektronen-Synchrotron, Hamburg.

Carlsten, B. E. (1989).New photoelectric injector design for the Los Alamos National Laboratory XUV FEL accelerator, *Nuclear Instrument and Methods* A 285, 313.

Cialdi, S.; Vicario, C.; Petrarca, M.; and Musumeci, P. (2007). Simple scheme for ultraviolet time-pulse shaping, *Applied Optics* 46, 4959.

Cornacchia, M. et al. (1998). *Linac Coherent Light Source (LCLS) Design Study Report*, SLAC Report No. SLAC-R-521, Stanford Linear Accelerator Center, Stanford.

Dickey, F M. & Holswade, S. C. (2000). *Laser Beam Shaping*, Marcel Dekker. Inc, New York,

Dromey, B.; Zepf, M.; Landreman, M.; O'Keeffe, K.; Robinson, T.; & Hooker, S. M. (2007). Generation of a train of ultrashort pulses from a compact birefringent crystal array, *Applied Optics* 46, 5142.

Goodman, J. W. (1985). *Statistical Optics*, John Wiley & Sons, New York.

Grunner, S. M. et al. (2002). Energy recovery linacs as synchrotron radiation sources, *Review of Scientific Instrument* 73, 1402.

Hoffnagle, J.A. & Johnson, C.M. (2000). Design and Performance of a Refractive Optical System that Converts a Gaussian to a Flattop Beam, *Applied Optics* 39, 5488.

Hill, K. B.; Purchase,K. G. & Brady, D. J. (1995). Pulsed-image generation and detection, *Optics Letters* 20, 1201.

Kempe, M.; Stamm, U.; Wilhelmi, B. & Rudolph, W. (1992). Spatial and temporal transformation of femtosecond laser pulses by lenses and lens systems, *Journal of the Optical Society of America* B9, 1158.

King, W. E. et al. (2005). Ultrafast Electron Microscopy in Materials Science, Biology, and Chemistry, *Journal Applied Physics* 97, 111101.

Kopp, A.; Ravel, L. & Meyrueis, P. (1999). Efficient beam shaper homogenizer design combining diffractive optical elements, microlens array, and random phase plate, *Journal of Optics* A1, 398.

Li, Y. & Crowell, R. (2007). Shortening of laser pulse with self modulated phase at the focus of a lens, *Optics Letters* 32, 93.

Li, Y. & Chemerisov, S. (2008). Manipulation of spatiotemporal photon distribution via chromatic aberration, *Optics Letters* 33, 1996.

Li, Y. & Lewellen, J. W. (2008). Generating quasi-ellipsoidal electron beam by 3-D laser pulse shaping, *Physical Review Letters* 100, 074801.

Li, Y.; Chemerisov, S. & Lewellen, J. W. (2009). Laser pulse shaping for generating uniform three-dimensional ellipsoidal electron beams, *Physical Review ST AB* 12, 020702 (2009).

Limborg-Deprey, C. & Bolton, P. (2006) *Nuclear Instrument and Methods* A 557, 106 (2006).

Luiten , O. J.; van der Geer, S. B.; de Loos, M. J.; Kiewiet, F. B. & van der Wiel, M. J. (2004). How to Realize Uniform Three-Dimensional Ellipsoidal Electron Bunches, *Physical Review Letters* 93, 094802.

Musumeci, P. J.; Moody, T.; England, R. J.; Rosenzweig, J. B. & Tran, T. (2008). Experimental Generation and Characterization of Uniformly Filled Ellipsoidal Electron-Beam Distributions, *Physical Review Letters* 100, 244801.

Nuss, M. C. & Morrison, R. L. (1995). Time-domain images, *Optics Letters* 20, 740.

Piestun R. & Miller, D. A. B. (2001). Spatiotemporal control of ultrashort optical pulses by refractive–diffractive–dispersive structured optical elements, *Optics Letters* 26, 1373.

Reiser, M. (2005). *Theory and Design of Charged Particle Beams*, Wiley, New York.

Serafini, L. & Rosenzweig, J. B. (1997). Envelope analysis of intense relativistic quasilaminar beams in rf photoinjectors:mA theory of emittance compensation, *Physical Review* E 55, 7565.

Sharma, A. K.; Tsang, T. & Rao, T. (2009). Theoretical and experimental study of passive spatiotemporal shaping of picosecond laser pulse, *Physical Review* ST AB 12, 033501.

Sider, C. (1998). Pulse-Train Generation Using a 2 n-Pulse Michelson Interferometer, *Applied Optics* 37, 5302.

Stuart, B. C.; Feit, M. D.; Rubenchik, A. M.; Shore,;B. W. & Perry, M. D. (1995). Laser-Induced Damage in Dielectrics with Nanosecond to Subpicosecond Pulses, *Physical Review Letters* 74, 2248.

Taylor, A. J.; Rodriguez, G. & Clement, T. S. (1996). Determination of n2 by direct measurement of the optical phase, *Optics Letters* 21, 1812.

Tien, A.-C.; Backus, S.; Kapteyn, H.; Murnane, M. & Mourou, G. (1999). Short-Pulse Laser Damage in Transparent Materials as a Function of Pulse Duration, *Physical Review Letters* 82, 3883.

Tomizawa, H.; Dewa, H.; Taniuchi, T.; Mizuno, A.; Asaka, T.; Yanagida, K.; Suzuki, S.; Kobayahsi, T.; Hanaki, H. & Matsui, F. (2006). Adaptive shaping system for both spatial and temporal profiles of a highly stabilized UV laser light source for a photocathode RF gun, *Nuclear Instrument and Methods* A 557, 117.

Vaughan, J.C.; Feurer, T. & Nelson, K. A. (2002). Automated two-dimensional femtosecond pulse shaping, *Journal of the Optical Society of America* B 19, 2489.

Veetil, S.P.; Vijayan, C. D.; Sharma, K.; Schimmel, H. & Wyrowski, F. (2006). Diffraction induced space-time splitting effects in ultra-short pulse propagation, *Journal of Modern Optics* 53, 1819.

Verluise, F.; Laude, V.; Cheng, Z.; Spielmann, Ch.; & Tournois, P. (2000). Amplitude and phase control of ultrashort pulses by use of an acousto-optic programmable dispersive filter: pulse compression and shaping, *Optics Letters* 25, 575.

Weiner, A. M. (1995). Femtosecond Optical Pulse Shaping and Processing, *Progress in Quantum Ellectronics* 19, 161.

Weiner, A. M. (2000). Femtosecond pulse shaping using spatial light modulators, *Review of Scientific Instrument* 71, 1929.

Welford, W.T. (1960). Use of Annular Apertures to Increase Focal Depth, *Journal of the Optical Socity of America* 50, 749.

Will, B. I. & Klemz, G. (2008). Generation of flat-top picosecond pulses by coherent pulse stacking in a multicrystal birefringent filter, *Optics Express*, 16, 14922.

Yang, J.; Sakai, F.; Yanagida, T.; Yorozu, M.; Okada, Y.; Takasago, K.; Endo, A.; Yada, A. & Washio, M. J. (2002). Low-emittance electron-beam generation with laser pulse shaping in photocathode radio-frequency gun, *Applied Physics* 92, 1608.

Zhang, S.; Neil, G. & Shinn, M. (2003). Single-element laser beam shaper for uniform flat-top profiles, *Optics Express* 11, 1942.

Zhou, C. S. et al. (2007). Efficient temporal shaping of ultrashort pulses with birefringent crystals, *Applied Optics* 46, 1 - 5.